ELSEVIER

Polymer 43 (2002) 1907–1913

polymer

www.elsevier.com/locate/polymer

X-ray diffraction study of the structure of thin polyfluorene films

S. Kawana[a,*], M. Durrell[b], J. Lu[b], J.E. Macdonald[b], M. Grell[c], D.D.C. Bradley[c], P.C. Jukes[c], R.A.L. Jones[c], S.L. Bennett[d]

[a]*Cavendish Laboratory, University of Cambridge, Madingley Road, Cambridge CB3 0HE, UK*
[b]*Department of Physics and Astronomy, University of Wales Cardiff, PO Box 913, Cardiff CF2 3YB, UK*
[c]*Department of Physics and Astronomy, University of Sheffield, The Hicks Building, Hounsfield Road, Sheffield S3 7RH, UK*
[d]*CLRC Daresbury Laboratory, Warrington, Cheshire WA4 4AD, UK*

Received 23 April 2001; received in revised form 30 August 2001; accepted 11 September 2001

Abstract

The molecular arrangement in thin films of poly(9,9-dioctylfluorene) and poly(9,9-dihexylfluorene) deposited on silicon substrates has been investigated with grazing incidence X-ray diffraction. In particular, the effect of the interface on the molecular orientation is highlighted. Both materials display a periodicity normal to the surface arising from stacked sheets of fluorene chains in both the crystalline and liquid crystalline phases. For the crystalline phase, a periodicity in the plane of the surface of 4.15 Å is observed corresponding to half the fluorene ring repeat distance along the backbone, consistent with interdigitating side-chains. For crystalline films deposited onto rubbed polyimide films, strong orientation effects are observed. In the liquid-crystalline phase, this strong in-plane ordering of backbones is lost. Poly(9,9-dihexylfluorene) exhibits an additional degree of ordering in the plane of the interface, which is likely to arise from hexagonal ordering of the backbone chains.

Keywords: Polyfluorene; Grazing incidence X-ray diffraction; Thin films

1. Introduction

Polyfluorenes (PFOs) are conjugated polymers which have been reported to show efficient blue electroluminescence (EL) [1]. Fluorene homo- and copolymers have attracted intense interest for their potential applications in organic light emitting diodes (OLEDs), organic thin film transistors, and light-emitting electrochemical cells [1–5]. As for most conjugated polymers, the molecular architecture is that of a rigid, rod-like polymer backbone with flexible side chains ('hairy rods'). 'Hairy rod' polymers have long been studied and are widely known for their liquid crystalline (LC) behaviour [6]. It was not surprising, therefore, that for poly(paraphenylene vinylene) (PPV) and related conjugated 'hairy rods', LC behaviour was reported [7,8] soon after the first report on polymer electroluminescence (EL) from PPV [9]. From aligned ensembles of conjugated polymers, one expects polarised luminescence as well as high charge carrier mobilities; consequently the existence of LC phases providing such alignment by self-organisation is an asset for polymer semiconductors. However, for LC PPVs, alignment was found to be fragmented into a typical 'domain' structure, which is the LC analogue to a polycrystalline material. In such a domain structure, no macroscopically anisotropic behaviour results. No alignment of LC PPV films, or indeed any other 'hairy rod' polymer, into macroscopic 'mono domains'—the LC analogue for single crystals—has been reported.

The discovery [10] that the poly(9,9-dioctylfluorene) (F8) not only displays a 'hairy rod' LC phase, as well, but that thin F8 films in their LC phase can be aligned into monodomains with the help of the standard alignment technique employed for low molecular weight LCs, namely annealing on a rubbed polymer substrate, has paved the way towards the exploitation of the LC properties of conjugated polymers in OLEDs with an architecture similar to the standard OLED design. Polarised EL devices from LC PFOs were reported soon thereafter [11,12], and the later report of monodomain alignment of fluorene copolymers in a similar fashion [13] has found application for high-mobility thin film transistors [3,4].

The question why PF LCs tend to align on conventional alignment layers, while other 'hairy rods' do not, has led to a desire for a more detailed understanding of PFO morphology and phase behaviour. This desire was reinforced by

* Corresponding author. Present address: Yokohama Research Centre, Mitsubishi Chemical Corporation, 1000 Kamoshida, Yokohama 227-8502, Japan. Tel.: +81-45-963-4223; fax: +81-45-963-4438.
E-mail address: kawana@rc.m-kagaku.co.jp (S. Kawana).

0032-3861/02/$ - see front matter
PII: S0032-3861(01)00753-4

another intriguing observation, that the photophysical properties of F8, namely its absorption, photoluminescence (PL) and EL spectra, display a complex dependence on their physicochemical treatment history [10,14,15]. X-ray fibre diffraction studies on F8 fibres that had undergone either thermal crystallisation or prolonged solvent exposure, or both, have helped to elucidate the underlying structure–property relationships [16]. However, the structural characterisation of F8 cannot be seen as complete until two remaining questions are clarified: firstly, the precise unit cell of crystalline F8 has so far not been reported, and secondly, the structures seen by diffraction from bulk fibres (~1–2 mm diameter) may differ significantly from those occurring in thin films, which are more relevant for photophysical behaviour and applications. The latter of these points has recently been addressed by thin film electron diffraction studies on a closely related material [17], which have in particular provided a more precise picture of the backbone planarisation. They found that the polymer backbone takes a 5_2 helix structure.

In the present paper, we report grazing-incidence X-ray diffraction (GIXRD) studies on thin F8 and poly(9,9-dihexylfluorene) (F6) films, aiming in particular at clarifying the arrangement of the chain backbone and flexible side-chains with respect to the substrate, as a result of the geometrical constraints in association with the contribution from the interface/surface energy.

GIXRD is well suited for structural studies of thin films and surfaces. By employing an angle of incidence α less than the critical angle α_c (typically of the order of 0.2°), the penetration of the X-ray beam can be limited to 50 Å or so, giving surface sensitivity to the topmost polymer molecules at the surface. Larger values of α lead to diffraction patterns for the bulk of the thin film. Most GIXRD studies have concentrated on semiconductor and metal surfaces, in vacuum, in gaseous atmospheres and under liquid films. Factor et al. pioneered the application of GIXRD to polymer films [18]. They investigated the near surface structure of aromatic polyimide films as a function of thermal treatment and film thickness. The structure parallel to the film surface was found to be more ordered at the air surface than bulk for the thick film. Recently, Sirringhaus et al. have employed this technique to investigate the molecular arrangement in the bulk of conjugated polymer, poly(3-hexylthiophene) thin films [19].

In this paper, we will report molecular ordering structures in thin PFO films, which had been annealed at temperatures above and below the melting point T_m followed by quenching to room temperature so that the structure would be frozen. The ordering with respect to both the axis normal and parallel to the substrate surface have been investigated. In addition, the influence of the side chain length and of deposition onto a polyimide alignment layer on the resulting structure will be reported.

2. Experimental

For the most part of this study, poly(9,9-dioctylfluorene), whose chemical structure is shown in Fig. 1, was used. This is the same material as one used in previous studies by Grell et al. [10,12,15,16] and the details are described therein. We will refer to this material as F8 in this paper. We also used poly(9,9-dihexylfluorene) (F6) to examine the effect of shorter side-chains on the structure. In combined differential scanning calorimetry (DSC) and polarisation microscope studies during heating of an amorphous film [10], F8 was found to exhibit a crystallisation peak at $T_c \approx 80$ °C and a melting endothermal peak at $T_m \approx 157$ °C at the heating rate of 20 °C/min. Since PFO is a rigid-rod-like polymer, almost perfect crystallisation can be achieved, unlike typical semi-crystalline polymers. Above this temperature, the PFO is a birefringent liquid crystalline melt, which becomes isotropic at $T_I \approx 270$–280 °C. This transition to the isotropic phase was found to be reversible. Importantly crystallisation was found to be prevented almost entirely by rapid cooling from a melt state leading to a glassy state. For F6, T_m is about 200 °C and T_I is above 300 °C, also determined by DSC.

Film samples were prepared by spin coating from 10 g/l toluene solutions at 2000 rpm onto bare 5-mm-thick silicon substrates. The silicon substrate had not undergone any surface treatment and thus films were deposited on a native oxide layer after cleaning by NH_4OH(4.3%w/w)/H_2O_2(4.2%w/w) aqueous solution at 75 °C for 10 min to remove organic impurities prior to spin coating. F8 layers were also spin cast onto a polyimide alignment layer, which had been deposited on silicon substrates and rubbed in advance. The thicknesses of the resulting films were 50 nm determined by two methods; the spectroscopic ellipsometry (Jovin–Yvon, France) and the surface profile tracer (Dektak styrus profiler, USA). Films were then annealed at several temperatures below and above T_m on a hot stage (Linkham, UK) in air. No structural differences were observed between samples annealed on the hot stage and those annealed in a vacuum oven. After being annealed for 30 min, films were quenched to room temperature in order to freeze the sample structure for X-ray measurements under ambient conditions, as described in Ref. [10].

Measurements were taken on the XMaS beamline at the European Synchrotron Radiation Facility (ESRF),

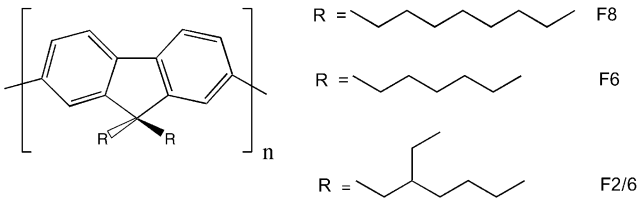

Fig. 1. The chemical structure of PFO. Note that the fluorene unit is planar and the side alkyl chains are in a plane perpendicular to the fluorene unit [20].

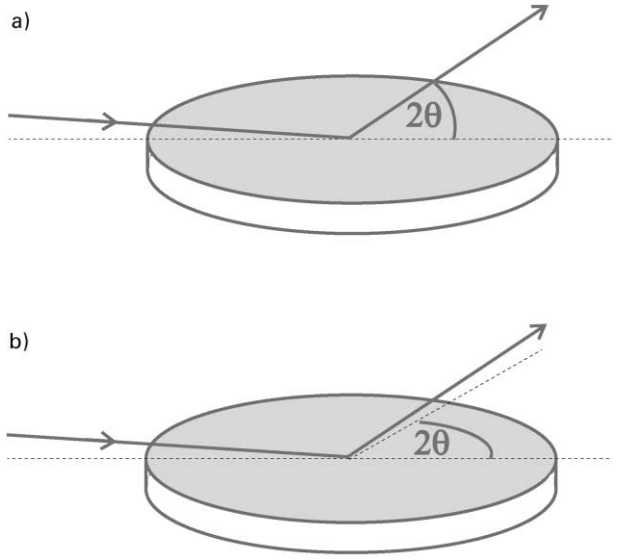

Fig. 2. Scattering geometries employed. (a) Grazing incidence asymmetric Bragg scattering (GIABS) geometry, in which the scattering vector $\boldsymbol{Q}$ has a large component ($\approx Q\cos\theta$) normal to the surface. (b) Grazing incidence surface plane scattering (GISPS) geometry, in which the $\boldsymbol{Q}$ is in the plane of the surface for $\alpha \approx \alpha_c$. This is the conventional geometry for GIXRD surface studies.

Grenoble, France and Station 9.4 at the Synchrotron Radiation Source (SRS), Daresbury, UK. Both instruments use a channel-cut Si(111) monochromator crystal with a toroidal mirror. The wavelength was set to 1.60 Å at SRS, while, at ESRF, a relatively long wavelength, $\lambda = 2.48$ Å, was used in order to minimise beam damage to the samples, which was significant at short wavelengths. The beam size of 3×0.5 mm was defined by four-jaw slits before the sample. Two sets of four-jaw slits on the detector arm were used to define the resolution and the surface area on the sample from which scattered radiation was collected by a Ge solid state detector. An air-filled ion chamber located just before the sample was used as a monitor for the incident beam flux.

Two scattering geometries were used to investigate the structure of the bulk of the film. In the grazing incidence asymmetric Bragg scattering (GIABS) geometry, the scattering vector $\boldsymbol{Q}$ is defined by the incident and (much larger) exit beam angles (see Fig. 2a). This gives information primarily about correlations normal to the sample surface although $\boldsymbol{Q}$ has a significant in-plane component. In the grazing incidence surface-plane scattering (GISPS) geometry, the exit angle is kept equal to the (small) incident angle. The scattering vector is primarily defined by the azimuthal displacement of the exit beam, hence, giving information about correlations parallel to the sample surface (see Fig. 2b). The alignment of the F8 molecules on the polyimide substrate was investigated by fixing the incident and exit angles (in both geometries) and rotating the sample azimuthally. The angle of incidence α was set just above the critical angle α_c to ensure the beam penetrated the whole film. The measuring time depends on the intensity of the incident beam. A typical count-time for one data point was set to 20 s at SRS, and to 1 s at ESRF for both GIABS and GISPS geometry.

3. Results

We present results of X-ray diffraction measurements in GISPS and GIABS geometries for the phases of F8 and F6 determined by Grell et al. [10]. The effect of polyimide alignment layers on the ordering of F8 overlayers is also described.

3.1. The crystalline phase on a non-aligned substrate

F8 and F6 samples were annealed at 130 and 170 °C, respectively, for 30 min in order to obtain the crystalline phase and quenched to room temperature. Scans in the GIABS geometry are shown in Fig. 3. Strong Bragg peaks were observed for F8 and for F6 at $|\boldsymbol{Q}| = 0.491$ and 0.596 Å^{-1}. The component of $\boldsymbol{Q}$ normal to the interface $Q_1 = 0.490$ and 0.583 Å^{-1} for F8 and F6 correspond to d-spacings normal to the interface of 12.8 and 10.8 Å, respectively. Scans in the GISPS geometry for F8 and F6 are shown in Fig. 4 as a function of $Q_{/\!/}$, the component of $\boldsymbol{Q}$ parallel to the surface. In this geometry, we also observed one clear peak for F8 at $Q_{/\!/} = 1.497$ Å^{-1} corresponding to a d-spacing of 4.19 Å, whereas two distinct peaks were observed for F6 at $Q_{/\!/} = 1.514$ and 1.001 Å^{-1} corresponding

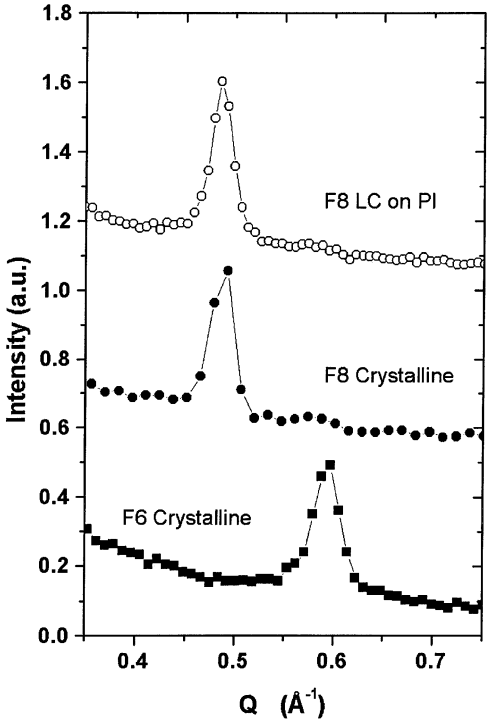

Fig. 3. Scans in the GIABS geometry for F8 and F6 in the crystalline phase on non-aligned substrates, and F8 in the liquid crystalline phase on an alignment layer. The profiles are offset vertically for clarity.

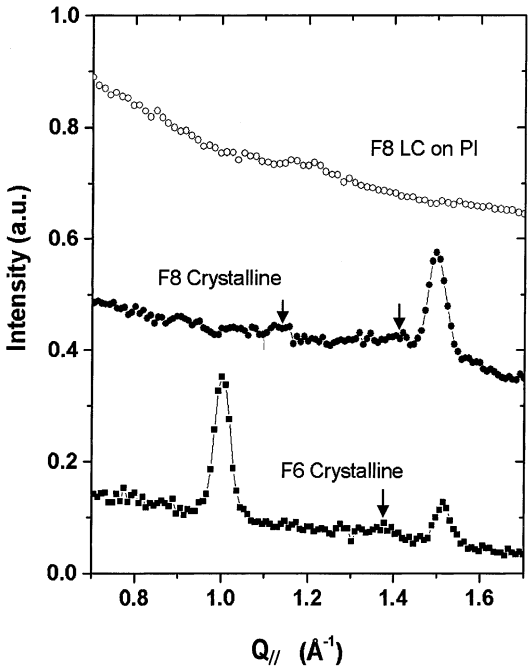

Fig. 4. Scans in the GISPS geometry for F8 and F6 in the crystalline phase on non-aligned substrates, and F8 in the liquid crystalline phase on an alignment layer. The profiles are offset vertically for clarity. Arrows indicate very weak peaks at $Q_{//} \approx 1.13$ Å^{-1} (for F8 only) and $Q_{//} \approx 1.40$ Å^{-1} (common to F6 and F8).

to a d-spacing of 4.16 and 6.23 Å, respectively. It should be noted these GISPS peaks are observed only when the incident angle is close to the critical angle and, hence, that these in-plane peaks arise from ordering parallel to the surface. In addition to these major peaks, very weak peaks are observed consistently at 1.40 and 1.13 Å^{-1} for F8, whereas one weak peak is observed at 1.40 Å^{-1} for F6, as are indicated by arrows in Fig. 4. These weak peaks will not be discussed further since we have performed all scans under grazing incidence conditions scanning a limited part of reciprocal space. Further experiments are planned to probe a large volume of reciprocal space with area detectors in time-resolved mode during in-situ annealing in a vacuum furnace for a range of relevant processing conditions. Here we concentrate on the major peaks observed to shed light on the chain architecture in the PFO thin films and on the effect of the interface on the structure, as compared with the bulk structure as obtained for X-ray fibre diffraction [16].

In determining the molecular orientation in the crystalline film, certain aspects become immediately apparent from consideration of the major peaks in the scans.

1. Peaks are observed in the GISPS geometry at approximately the same Q value for both F6 and F8 at

   $Q_{//} = 2\pi/d = 1.50$ Å^{-1}.

   These peaks can be identified with the benzene ring repeat distance along the polymer chain $a_{\text{benzene}} = 4.15$ Å. (This benzene ring repeat distance is half the fluorene monomer repeat distance.) Hence, we can infer that the polymer backbone lies in the plane of the surface. In their fibre diffraction study of F8, Grell et al. observed the meridional peak at the same Q value, which, according to their model, is attributed to packing of intercalated side chains of neighbouring polymer backbones displaced along their length by half a fluorene ring repeat distance ($a_{\text{fluoerene}} = 8.3$ Å) [16]. We are of the opinion that this is the likely cause of the common peak observed for F8 and F6 at $Q_{//} \approx 1.50$ Å^{-1} in the GISPS geometry as shown in Fig. 4. We calculate the correlation length from the width of these peaks on the basis of exponentially-decaying correlations, for which the correlation length is given by 1/HWHM (half width at half maximum). The observed peak widths correspond to the correlation lengths of 44 Å (F8) and 50 Å (F6).
2. In the GIABS geometry, two different periodicities are observed for the two materials: 10.8 Å for F6 and 12.8 Å for F8. From this we can conclude that the spacing between polymer chains normal to the surface is governed by the length of the side-chains, which is about 8 Å for F6 and 10 Å for F8. This is in agreement with our earlier inference that the F8 backbone lies in the plane of the surface. Thus, we propose a basic structure in which the backbone of the polymer chains lie in the plane of the interface, with interdigitation of partially overlapping side-chains at neighbouring backbones over a length-scale of the order of the persistence length, as shown in Fig. 5.
3. For F6, the scans in the GISPS geometry reveal an additional peak at $Q_{//} = 1.001$ Å^{-1}, which is not observed in F8. The origin of this peak will be discussed later. It is likely to arise from inter-chain correlations in the plane of the surface that occur in F6 but not in F8.

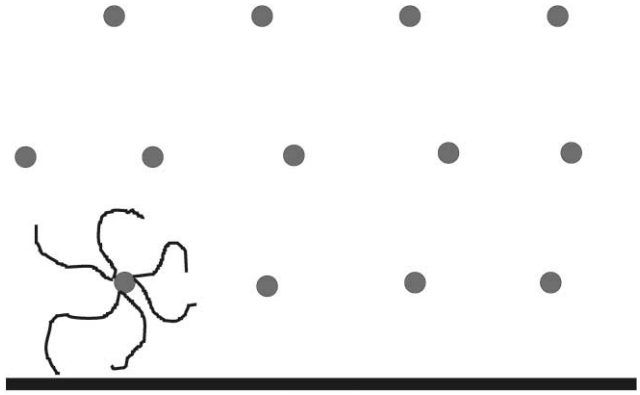

Fig. 5. Schematic structure for F8 in the crystalline phase. Short lengths of F8 chains are viewed end-on. In the LC phase, the layering persists but the chains do not order strongly in the in-plane direction.

3.2. The structure of the LC phase of F8

In order to study the LC phase structure, an F8 film was

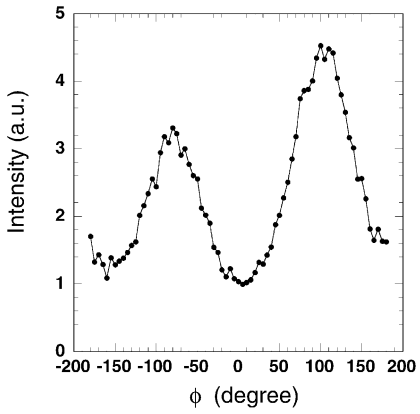

Fig. 6. The peak intensity at $Q_{/\!/} = 1.50$ Å^{-1} in the GISPS geometry (shown in Fig. 4 for an unaligned sample) for F8 in the crystalline phase as a function of azimuthal angle ϕ; $\phi = 0$ approximately corresponds to the condition when the rubbing direction is parallel to the in-plane component of the incident beam vector.

annealed at 180 °C followed by quenching to room temperature to freeze the structure. GIABS scans with the incident angle greater than the critical angle were carried out on this film in the same manner as stated above. In the GIABS geometry, peaks are again observed at $Q = 0.490$ Å^{-1} for F8, which is the same value as for the corresponding crystalline phase. The major peaks observed in scans in the GISPS geometry for F8 and F6 in the crystalline phase are absent in the LC phase. The structure of F8 in the LC phase can thus be explained also by the model shown in Fig. 5 but without the ordering of chains in the plane of the surface as occurs in the crystalline phase.

3.3. The structure of F8 film on an alignment layer

In order to investigate the effect of an alignment layer, F8 films were spin cast onto a rubbed polyimide (PI) film deposited onto a silicon substrate and annealed at 130 °C to form the crystalline phase. We observed peaks at the same Q-values as for the crystalline phase for both scattering geometries confirming that the alignment layer does not affect the nature of the structure in the crystalline phase. The effect of the PI alignment layer on the orientation of the crystalline structure was probed by azimuthal scans through the crystalline peaks. The result for the GISPS peak is shown in Fig. 6, where ϕ approximately corresponds to the angle between the in-plane component of incident beam vector and the rubbing direction (set by eye). Since $2\theta = 22.15°$ for the GISPS peak (Fig. 2b) for $\lambda = 1.60$ Å, $\phi \approx -79$ and 101° correspond to the conditions when $Q_{/\!/}$ is parallel to the rubbing direction. The observed values at which the maximum intensities occur are close to these ϕ's, indicating that this GISPS peak arises from a repeating distance along the polymer backbone. It should be noted that, since the scattering intensity is very sensitive to α when $\alpha \approx \alpha_c$, a small misalignment of the sample results in a relatively large difference in the scattering intensity. This is probably responsible for the difference in the intensities between two maxima, and thus, it is difficult to discuss details of the ϕ-dependence of the GISPS peak intensity. However, it is clear from this result that the majority of backbone chains lie in the direction of rubbing as can be inferred from the optically determined order parameter, $S = 0.65$ [10]. The correlation length estimated from the peak widths at these maxima is 175 Å, which is about three times larger than that of non-aligned samples. This value is quite close to the fibre diffraction result, 150 Å, for the F8 fibre sample that had been drawn from nematic melt followed by thermal crystallisation [16].

For the LC phase on a PI alignment layer prepared by the same thermal history as above, GISPS scan with the incident angle near the critical angle shows a halo centered at $Q_{/\!/} = 1.18$ Å^{-1} ($d = 5.3$ Å) (Fig. 4). It should be noted that this halo is not observed for the LC phase sample without an alignment layer. No distinct peak is observed in the GISPS scattering geometry for LC phase regardless of the existence of an alignment layer. The origin of this halo is unclear.

4. Discussion

The main structural features observed may be summarised as follows:

1. For the crystalline and LC phases, the structure is periodic normal to the interface with a periodicity of 12.8 Å for F8 and 10.8 Å for F6. This strongly suggests that this periodicity is governed by the alkyl side-chain length.
2. Scans in the GISPS geometry for the crystalline phase, reflecting correlations in the plane of the surface, show a peak for both F8 and F6 at $Q = 1.499$ and 1.512 Å^{-1}, respectively, which closely corresponds to the phenyl ring distance 4.15 Å. This peak is consistent with interdigitation of side-chains of neighbouring chains. An additional peak is observed for F6 at $Q = 1.001$ Å^{-1}, the origin of which is discussed below.
3. Deposition of F8 films on a pre-aligned PI layer causes preferential alignment of the chains. For the crystalline phase, the intensity of the GISPS peak at 1.50 Å^{-1} is maximized when $Q_{/\!/}$ is along the rubbing direction as expected, since this peak corresponds to periodicity along the chain direction. For the LC phase of F8 on the PI alignment layer, there is weak molecular ordering in the plane of interface with a periodicity of 5.3 Å. This peak is also observed for F8 crystal, though the intensity is weak, but not for F6.

The structure of F8 consists of layers of fluorene backbones, which are periodic normal to the substrate, the spacing between which is determined by the side-chain length. In the LC phase without an alignment layer, there is no macroscopic ordering of the backbones in the plane of the surface that can be detected with GIXRD. Weak in-plane

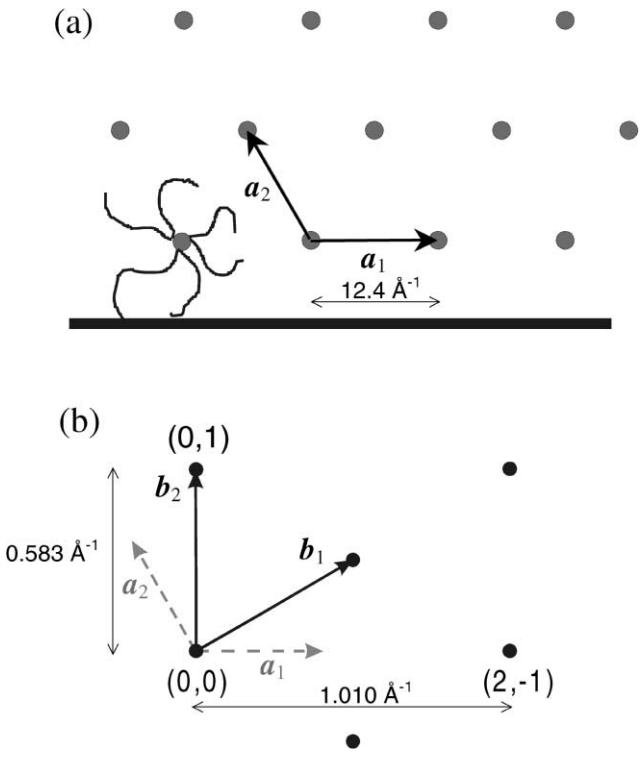

Fig. 7. (a) Schematic structure for the crystalline phase of F6 thin films, showing the hexagonal unit cell vectors, $\boldsymbol{a}_1$ and $\boldsymbol{a}_2$ (in two dimensions) and its orientation with respect to the interface. (b) The corresponding reciprocal lattice vectors, $\boldsymbol{b}_1$ and $\boldsymbol{b}_2$. The lowest-angle reciprocal lattice point in the plane of the interface is (2, − 1), occurring at $Q_{/\!/} = 1.01$ Å^{-1}, whilst the lowest-angle reciprocal lattice point normal to the interface is (0,1), occurring at $Q_{\perp} = 0.583$ Å^{-1}.

ordering is detected for the LC phase when deposited onto a PI alignment layer. In the crystalline phase, an additional periodicity of 4.15 Å is detected in the plane of the interface, which can be identified with the benzene ring periodicity. This is consistent with interdigitation of side-chains.

The structure of F6 in the liquid crystalline phase is analogous to that observed for F8 except for the reduced spacing between layers as a result of the shorter side-chains. The crystalline phase is rather similar to that occurring in F8 except for the presence of an additional peak at 1.001 Å^{-1} corresponding to a d-spacing of 6.28 Å. No corresponding lower-order diffraction peaks are observed at lower Q-values. This spacing is too short to arise from a periodicity along the backbone, such as a helical conformation. Since it is substantially shorter than the alkyl side-chains, this spacing is also too short to be a first order peak from correlations between backbones. We postulate hexagonal ordering of the backbones as in Fig. 7(a), as has been observed for a close relative of F6, poly(9,9-bis(2-ethylhexyl)fluorene) F2/6, in which both hexyl side-chains per monomer are each replaced by branched 2-ethylhexyl chains [17]. Since it is most likely that the interface with the silicon substrate defines one axis of the hexagonal unit cell, we may define the unit cell vectors, $\boldsymbol{a}_1$, $\boldsymbol{a}_2$ and $\boldsymbol{a}_3$ as depicted in Fig. 7(a) for which $|\boldsymbol{a}_1| = |\boldsymbol{a}_2| = 12.4$ Å. The corresponding reciprocal lattice vectors, $\boldsymbol{b}_1$, $\boldsymbol{b}_2$ and $\boldsymbol{b}_3$ are defined by $\boldsymbol{b}_1 = 2\pi\boldsymbol{a}_2 \times \boldsymbol{a}_3/v_c$ etc. where v_c is the volume of the unit cell, and are shown in Fig. 7(b) in two-dimensions. We can thus identify the first reciprocal lattice point which lies in the $Q_{\perp} = 0$ plane, the (2, − 1) reciprocal lattice point, which occurs at $Q_{/\!/} = 1.010$ Å^{-1} close to the location of the observed peak at $Q_{/\!/} = 1.001$ Å^{-1}. The first reciprocal point normal to the surface, on the other hand, is the (0,1) point and is close to the location of the observed GIABS peak at $Q_{\perp} = 0.583$ Å^{-1}. This correspondence, together with the lack of viable alternative explanations for the origin of this additional peak in F6, suggests that there is hexagonal ordering of the backbones in the crystalline phase of F6 that does not occur in F8. The existence of stronger in-plane ordering in F6 is supported by the observation of a larger dichroic ratio in F2/6 than in F8 [17]. It should be noted that the hexagonal unit cell parameters for F2/6 are 16.7 Å, which is larger than those of F6. This suggests that the addition of the ethyl branch to the side hexyl chains result in a further separation of two adjacent chains without perturbing the main structure.

Thin film geometry gives rise to strong geometrical constraints normal to the surface, which influences molecular arrangements along this direction in association with surface/interfacial energy. On the other hand, the molecular arrangement in the plane of the surface is predominantly governed by the interactions between neighbouring chains due to the lack of such boundary conditions. The absence of the corresponding hexagonal ordering in F8 indicates that the interactions between neighbouring chains are weaker in F8 than F6, consistent with the lower melting temperature for F8. The weakening of interactions for longer side-chains suggests that the ordering results from backbone interactions, presumably involving the π-electrons. Confirmation of this hexagonal ordering of the backbones in F6 awaits investigation of a greater portion of reciprocal space. The GIXRD studies of F8 are currently being extended to probe differences in the structure of the surface (top 50 Å) dynamically during in-situ annealing.

5. Conclusions

The molecular arrangement of F8 and F6 in a thin film geometry was studied by GIXRD technique. For both F8 and F6 in the crystalline phase, the polymer backbones are predominantly oriented in the plane of the surface with interdigitating side-chains. The backbones occur in layers where the periodicity normal to the surface is governed by the alkyl side-chain length. This layered structure also occurs in the liquid crystalline phase—however there is no appreciable ordering in the plane of the surface for this phase. The transition from crystalline to liquid-crystalline phases is hence viewed as a biaxial disordering of chains in the plane of the surface. The crystalline phase of F6 exhibits

an additional peak indicating additional ordering in the plane of the surface over that observed in F8—this seems to be caused by hexagonal ordering of the backbones but this conclusion awaits confirmation.

Acknowledgements

MD and PC acknowledge support from EPSRC (GR/M08516). MG acknowledges support from EPSRC (GR/M08011). We also thank the support staff at the SRS and at the XMaS beamline, designed and built by M. Cooper and W.G. Stirling. We thank Dr Mark Bernius and Dr Mike Inbasekaran of the Dow Chemical Company for the polyfluorene samples used in these experiments.

References

[1] Grice AW, Bradley DDC, Bernius M, Inbasekaran TM, Woo EP. Appl Phys Lett 1998;73:629.
[2] Setayesh S, Marsitzky D, Mullen K. Macromolecules 2000;33:2016.
[3] Sirringhaus H, Wilson RJ, Friend RH, Inbasekaran M, Wu W, Woo EP, Grell M, Bradley DDC. Appl Phys Lett 2000;73(3):406.
[4] Sirringhaus H, Kawase T, Friend RH, Shimoda T, Inbasekaran M, Wu W, Woo EP. Science 2000;290:2123.
[5] Yang Y, Pei Q. Polymer Preprints 1997;38(1):335.
[6] Ballauff M. Angew Chemie Int Ed Eng 1989;28(3):253.
[7] Martelock H, Greiner A, Heitz H. Macromol Chem 1991;192:967.
[8] Bao YuL, Cai Z, Angew R. Chem 1993;105:1392.
[9] Burroughes JH, Bradley DDC, Brown AR, Marks RN, Mackay K, Friend RH, Burn PL, Holmes AB. Nature 1990;347:539.
[10] Grell M, Bradley DDC, Inbasekaran M, Woo EP. Adv Mater 1997;9:798.
[11] Grell M, Knoll W, Lupo D, Meisel A, Miteva T, Neher D, Nothofer HG, Scherf U, Yasuda A. Adv Mater 1999;11:671.
[12] Whitehead KS, Grell M, Bradley DDC, Jandke M, Strohriegl P. Appl Phys Lett 2000;76:2946.
[13] Grell M, Redecker M, Whitehead KS, Bradley DDC, Inbasekaran M, Woo EP, Wu W. Liq Cryst 1999;26(9):1403.
[14] Bradley DDC, Grell M, Long X, Mellor H, Grice A, Inbasekaran M, Woo EP. Proc SPIE 1997;3145:254.
[15] Grell M, Bradley DDC, Long X, Chamberlain T, Inbasekaran M, Woo EP, Soliman S. Acta Polym 1998;49:439.
[16] Grell M, Bradley DDC, Ungar G, Hill J, Whitehead KS. Macromolecules 1999;32:5810.
[17] Lieser G, Oda M, Miteva T, Meisel A, Nothofer H-G, Scherf U, Neher D. Macromolecules 2000;33:4490.
[18] Factor BJ, Russell TP, Toney MF. Macromolecules 1993;26:2847.
[19] Sirringhaus H, Brown PJ, Friend RH, Nielsen MM, Bechgaard K, Langeveld-Voss BMW, Spiering AJH, Janssen RAJ, Meijer EW, Herwig P, de Leeuw DM. Nature 1999;401:685–8.
[20] Leclerc M, Ranger M, Belanger-Gariepy F. Acta Cryst 1998;C54:799.